X-(2) Modulator With 40-GHz Modulation Utilizing BaTiO3 Photonic Crystal Waveguides

Girouard, Peter David; Chen, Pice; Jeong, Young Kyu; Liu, Zhifu; Ho, Seng-Tiong; Wessels, Bruce W.

Published in:
I E E E Journal of Quantum Electronics

Link to article, DOI:
10.1109/JQE.2017.2718222

Publication date:
2017

Document Version
Peer reviewed version

$\chi^{(2)}$ Modulator with 40 GHz Modulation Utilizing $BaTiO_3$ Photonic Crystal Waveguides

Peter Girouard, Pice Chen, Young Kyu Jeong, Zhifu Liu, Seng-Tiong Ho, and Bruce W. Wessels

***Abstract*— Future telecommunication and data center networks as well as quantum optical communication systems will require optical modulators with wide bandwidths, large extinction, low operating voltage, and small size. We report the first quantitative demonstration of slow light enhancement of the electro-optic (EO) coefficient in a $\chi^{(2)}$ ferroelectric waveguide at microwave modulation frequencies. This is demonstrated in a compact (1 mm) photonic crystal device with a voltage-length product ($V_\pi \cdot L$) of 0.66 V-cm at 10 GHz and measured electro-optic modulation out to 40 GHz. A local enhancement factor of 12 and effective electro-optic coefficient of 900 pm/V is measured in the PC region at a wavelength of 1530 nm. By further optimizing the PC structure, devices with EO 3 dB bandwidths greater than 40 GHz and voltage-length product of 0.16 V-cm are predicted with 100 μm interaction length.**

***Index Terms*— Electro-optical devices, Photonic crystals, Waveguide modulators**

I. Introduction

A major challenge posed by the exponentially increasing demands for data transfer is the realization of compact EO modulators with wide EO bandwidths, low operating voltage, large extinction, and small footprint. High-speed and low-power devices are especially important in short-reach networks where the replacement of copper with optical interconnects is sought at shorter and shorter length scales [1]. At the same time, greater component density is also required in longer distance networks.

The distinct requirements for long-haul and short-reach networks have resulted in different material platforms and modulation mechanisms being investigated for each. Lithium niobate has been well-established as the standard material used for modulators in long-distance communications for decades [2]. These devices, however, are centimeters long, preventing the use of $LiNbO_3$ in shorter-reach networks that require higher density. Silicon free-carrier modulators have received great interest as candidates for short-reach networks due to the potential for integrating both driver electronics and photonic elements into a single CMOS-compatible platform [3]. It remains a major challenge, however, to achieve simultaneously large bandwidths, low voltages, and large extinction in a single device architecture with a sub-millimeter device length [3]. Modulators based on InP either require higher voltages than silicon if using the quantum confined stark effect or have lower modulation depths if using the band-filling effect [4].

Enhancement of optoelectronic device performance for both the $LiNbO_3$ and silicon platforms has been demonstrated utilizing photonic crystal (PC) slow light structures. In $LiNbO_3$, the tunability of the PC band edge has been investigated as a modulation mechanism [5-7]. A major challenge for the devices presented in [5-7] was weak overlap between the PC structure and the optical mode of the $LiNbO_3$ waveguides. This limitation has since been addressed by others using smart cut $LiNbO_3$ films [8, 9]; high-speed PC modulators using $LiNbO_3$, however, have not yet been demonstrated. Silicon free-carrier modulators with dispersion-engineered line defect PC waveguides have been demonstrated with a reduced driving voltage or device length [10-14] resulting from an enhancement in the phase delay proportional to the optical group refractive index [15]. Silicon PC modulators have been reported with 40 Gbps operation comparable to that achieved in the highest performing rib waveguide silicon modulators with an order of magnitude smaller footprint, demonstrating the effect of slow light in reducing the required modulator size [10, 14]; silicon modulators, however, still suffer from low extinction, which

This work was supported by the National Science Foundation through Grants No. ECCS-1201853 and IIP-1500222. This work made use of the Materials Processing and Microfabrication Facility supported by the MRSEC program of the National Science Foundation (DMR-1121262) at the Materials Research Center of Northwestern University. Focused ion beam milling was carried out at the Center of Nanoscale Materials (CNM) at Argonne National Laboratory, supported by the US Department of Energy, Office of Science, Office of Basic Energy Sciences, under contract No. DE-AC02-06CH11357. High-speed measurements were undertaken using Northwestern University Physics Instrumentation and Fabrication Facilities, supported by National Science Foundation under Award No. DMR-0960120.

B. W. Wessels is with Department of Materials Science and Engineering, Northwestern University, Evanston, IL 60208, USA (Phone: 847-491-3219; Fax: 847-491-7820; e-mail: b-wessels@northwestern.edu).

P. Girouard was with Department of Materials Science and Engineering, Northwestern University, Evanston, IL 60208, USA. He is now with DTU Fotonik, Lyngby, Denmark (e-mail: pgir@fotonik.dtu.dk).

P. Chen was with Department of Materials Science and Engineering, Northwestern University, Evanston, IL 60208, USA. He is now with Argonne National Laboratory, Lemont, IL 60439 (e-mail: pice.chen@anl.gov).

Young Kyu Jeong was with Department of Materials Science and Engineering, Northwestern University, Evanston, IL 60208, USA. He is now with Korea Institute of Industrial Technology, Gangneung, Republic of Korea (e-mail: immrc80@gmail.com).

Z. Liu is with Department of Materials Science and Engineering, Northwestern University, Evanston, IL 60208, USA (e-mail: zhifu-liu@northwestern.edu).

S. Ho is with Department of Electrical Engineering and Computer Science, Northwestern University, Evanston, IL 60208, USA (e-mail: sth@ece.northwestern.edu).

limits reach. Compared with the approaches taken thus far on $LiNbO_3$, the dispersion-engineered line defect waveguides on silicon offer the advantage of wideband optical operation for wavelength division multiplexing applications. Dispersion-engineered Si slot photonic crystal waveguides have been further used to enhance the effective EO coefficient using EO polymers, showing promise to reduce the voltage of $\chi^{(2)}$ modulators [16-19].

In this work, we demonstrate the first high bandwidth $\chi^{(2)}$ dispersion-engineered PC modulator using thin film $BaTiO_3$. In comparison with Si and InP electro-absorption modulators, $\chi^{(2)}$ modulators have an intrinsically wide optical bandwidth of operation and a greatly simplified structure. $BaTiO_3$ thin films have measured in-device effective EO coefficients that are more than 10 times larger than those of $LiNbO_3$ [20], enabling much smaller footprint and lower-voltage devices. We have previously demonstrated $BaTiO_3$ conventional modulators with 0.39 V-cm voltage-length product [21] which is nearly a factor of 2 smaller than the best reported for silicon conventional modulators [22]. Use of an epitaxial thin film ferroelectric material offers the advantages of strong overlap between the PC structure and optical waveguide mode, and lower microwave losses that enables higher EO bandwidths [23]. Previously we reported on a compact PC $BaTiO_3$ modulator that operated in the optical C band with an electro-optic response out to 50 GHz [24]. At a frequency of 100 Hz, clear enhancement of the EO effect was observed compared to a ridge waveguide modulator. The enhancement, however, was not quantified at modulation frequencies above 100 Hz. Here we report on a line defect PC $BaTiO_3$ modulator at technologically relevant microwave frequencies of 10-40 GHz using optical spectrum analysis to quantify the EO coefficient and its enhancement. An EO coefficient of 107 pm/V and a local enhancement factor of 12 in the PC region is measured at 30 GHz. Wideband optical operation in the C band (1530-1565 nm) is demonstrated with an effective in-device electro-optic coefficient between 114 and 134 pm/V. From measured microwave properties of the device, simulation indicates that devices with greater than 40 GHz EO 3 dB bandwidth and 0.16 V-cm voltage-length product are achievable in sub-millimeter long devices.

II. Slow Light Barium Titanate Phase Modulator

A schematic representation of the slow-light traveling-wave modulator is shown in Fig. 1 (a). Light is confined vertically by the $BaTiO_3$ film by refractive index guiding provided by the MgO substrate and Si_3N_4 ridge, the latter of which also provides horizontal confinement. The modulator is a composite structure consisting of a PC segment positioned in the center of a 1 mm long interaction region. A schematic of the cross-section of the PC device is shown in Fig. 1 (b). The multilayer structure was formed by first epitaxially growing a 500 nm thick $BaTiO_3$ film on a (100) oriented MgO substrate using metal organic chemical vapor deposition (MOCVD) and then depositing a 120 nm thick Si_3N_4 layer on top using plasma enhanced chemical vapor deposition. Barium titanate has a crystal symmetry of 4mm in its tetragonal phase, and its r_{51} component is much higher than r_{33} component. Our experimental setup takes advantage of this r_{51} component in the optical modulator. The waveguides are oriented along the [110] direction in order to use the large off-diagonal r_{51} electro-optic tensor element of all domains with polarization in the plane of the film. Details on the MOCVD growth technique [25, 26] and processing steps for fabricating the Si_3N_4 ridge waveguide and gold electrodes [24] are reported elsewhere. The ridge waveguide is 2 µm wide and supports a single mode for TE and TM polarizations. The PC waveguide consists of a hexagonal array of holes in the electro-optic medium with a single line of holes removed in the direction of light propagation, commonly referred to as a W1 structure [27]. The W1 structure was patterned via focused ion beam lithography onto a $Si_3N_4/BaTiO_3$ ridge waveguide (Fig. 1 (c)). A compromise between scattering losses and electro-optic coefficient enhancement was obtained by patterning a 37 µm long PC region. The tapered regions are not optimized for adiabatic coupling but introduce a more slowly varying effective refractive index compared to an abrupt interface between the ridge waveguide mode and the line defect mode. The tapered transition region consists of 40 unit cells with the holes displaced outward by $0.25a$ per row, where a is the lattice constant (530 nm). The cross-sectional profile of the fabricated holes shows a conical profile (Fig. 1 (d)), as has been observed previously for PC structures fabricated using the same technique on $BaTiO_3$ [24] and $LiNbO_3$ [28].

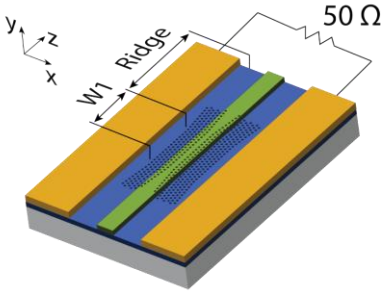

(a)

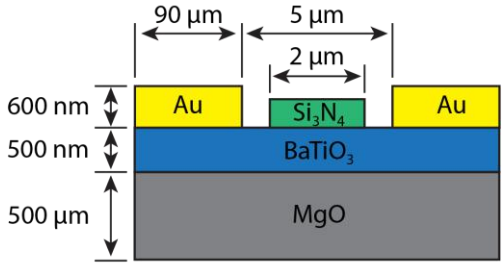

(b)

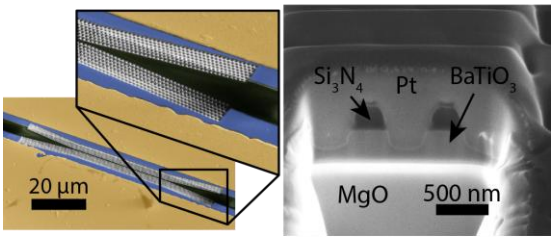

(c) (d)

Fig. 1. (a) Schematic of the photonic crystal modulator showing the W1 and ridge waveguide segments. (b) Cross-sectional diagram of the modulator showing the device geometry. (c) False-colored scanning electron microscope (SEM) image of the fabricated modulator with a magnified inset view of the tapered region. (d) Cross-sectional SEM image of the fabricated structure, showing a conical profile of the milled holes.

The waveguide was designed to have a low dispersion (LD) region in its optical group refractive index by shifting the first row of holes adjacent to the line defect [29] by $0.124a$, where a is the lattice constant of the photonic crystal. The band structure was calculated using the three-dimensional plane-wave expansion (PWE) method for modes having even symmetry with respect to the axis normal to the film top surface. This mode symmetry best represents the modes in the structure for incident TE polarized light. The top view of the supercell used for the simulations is shown at the top of Fig. 1 (a). The conical cross-sectional geometry of the holes used in the simulations was determined from the cross-section of fabricated structures, such as that shown in Fig. 1 (d).

The PhC structure of the Si_3N_4/BTO/MgO platform is asymmetric in the out-of-plane direction (y-direction in Fig. 1 (a)) due to asymmetric cladding materials above and below the waveguiding medium and conical shaped holes. Nonetheless, Qiu reported that with appropriate configuration, asymmetric PC slabs support lossless guided modes inside the band gap region [30]. Band gap effect exists in asymmetric PC slabs, but there are generally no separable non-interacting subsets of the modes.

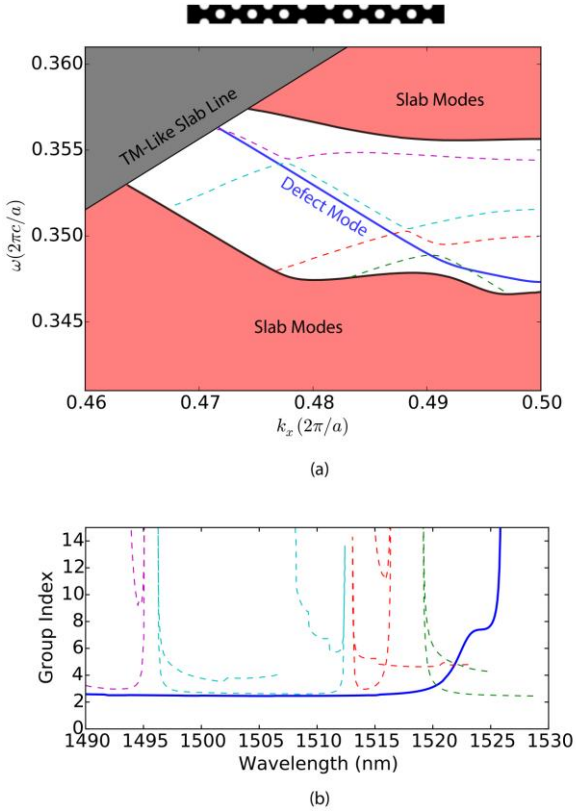

Fig. 2. (a) Band structure calculated using plane wave expansion in three dimensions. Shown above is the supercell used in the simulation. TM-like modes are dashed lines while the TE-like defect mode is a solid line within the band gap, shown as the white region. (b) Group refractive index of the line defect mode and TM-like modes calculated from the band diagram.

The asymmetry of the cladding and substrate and the non-cylindrical hole shape yield the complicated band structure shown in Fig. 2 (a). For an asymmetric slab, there are light cones corresponding to both cladding materials and an additional TM-like slab line, which is calculated from the band structure corresponding to TM-like modes of the unperturbed hexagonal lattice photonic crystal slab without the defect line [30]. The gap region is shown below the TM-like slab line in white. It is bordered by the regions of projected photonic crystal slab modes shaded red. The modes within the bandgap are distinguished by parity. A solid line indicates even (TE-like) parity, and dashed lines indicate odd (TM-like) parity. A single line defect mode with TE-like parity is within the gap region. Coupling from the TE-like defect mode to the TM-like modes is possible at crossings in the band diagram [31]. Additional coupling between TE-like and TM-like modes is possible at other points due to the large value of r_{51}.

Deflection into the substrate has previously been shown for $LiNbO_3$ PC waveguides fabricated in the same manner and having a similar conical hole geometry [28]. Since the calculated modes shown in Fig. 2 (a) all lie above the light line for the substrate, leakage of the guided modes into the substrate is likely a dominant optical loss mechanism. The PC length was chosen to prevent substantial leakage to the substrate while ensuring a long enough interaction length to unambiguously measure the electro-optic coefficient enhancement.

The corresponding optical group refractive index of the line defect mode is calculated as $n_g = c/(d\omega/dk)$, where c is the speed of light in free space, ω is the angular frequency, and k is the wavenumber. The group index is plotted versus wavelength in Fig. 2 (b) for the lattice constant of 530 nm which is also used in the fabricated structure. A low dispersion region of the TE-like mode with an average group index of 7.4 ± 0.74 within a 2 nm range centered at 1524.2 nm. The group indices of the TM-like modes are also calculated, showing a group index enhancement between 1495 and 1526 nm when TM-like modes are excited.

III. Microwave Properties

Due to the intrinsic microwave loss of the device, the microwave signal will be attenuated along its traveling path. The microwave losses consist of walk-off between the optical and microwave signals due to optical group refractive index and microwave refractive index mismatch, also reflections due to impedance mismatch to the 50 Ω system, and attenuation.

In order to accurately describe the phase modulated response at frequencies above 10 GHz, knowledge of the microwave losses are required. The dependence of the electro-optic frequency response on the microwave losses was investigated independently through electro-optic response modeling using microwave properties obtained from scattering-parameter measurements and electro-optic frequency response measurements with a calibrated vector network analyzer (VNA) setup as described in [24]. The microwave refractive index and characteristic impedance (Fig. 3 (a)) obtained from S-parameter measurements are flat over the range 18-50 GHz, attaining average values of 5.1 and 22

Ω, respectively. The resulting refractive index mismatch the optical mode with refractive index of 2.13 and impedance mismatch to the 50 Ω system are not negligible. The frequency-dependent total attenuation losses (Fig 3 (b)) were obtained from the measured S-parameters using the approach of Noguchi et al [33]. Fitting to the model $\alpha = \alpha_c\sqrt{f} + \alpha_d f$ gives conductor and dielectric loss coefficients of 9.2 dB/cm/$\sqrt{\text{GHz}}$ and 0.68 dB/cm/GHz, respectively. The large attenuation losses are primarily due to the high dielectric constant and large thickness of the $BaTiO_3$ film. The three types of losses can be reduced by both incorporating a low refractive index buffer layer between the electrodes and $BaTiO_3$ film [34] and by electroplating thicker electrodes with a wider gap [36]. An alternative approach is to use thinner $BaTiO_3$ films. Impedance matching to 50 Ω and an order of magnitude smaller conductor loss are simultaneously obtained in films with 260 nm thickness; however, the measured effective electro-optic coefficient is lower, requiring a larger slow light enhancement. Lumped element electrodes have comparable performance for devices using thick $BaTiO_3$ films and small gap spacing, but traveling-wave devices have larger bandwidths for devices using thinner $BaTiO_3$ films with larger electrode gap spacing. The thickness and gap dependent microwave and electro-optic properties will be discussed elsewhere [23].

The electro-optic intensity modulated frequency response was measured by operating the conventional phase modulator between crossed linear polarizers using the experimental setup described by Tang et al. [36]. For these measurements, both TE and TM polarizations with equal intensity were launched into the device. The electro-optically induced phase delay between the two polarization modes is converted to an amplitude response by passing through the second polarizer. The measured electro-optic intensity modulated frequency response is shown in Fig. 3 (c) as the blue solid curve. The traveling-wave device has a measured 3 dB EO bandwidth of 4.5 GHz with a measured response out to 40 GHz. The response was modeled using the approach of Haxha et al [35] and is shown as the red dashed curve in Fig. 3 (c). The measured frequency-dependent microwave refractive index, characteristic impedance, and attenuation losses were included in the model. Comparing the measured and modeled EO response, the model predicts a lower response at lower frequencies and a slightly higher response at higher frequencies than what is measured. This is attributed to a frequency dependence of the electro-optic coefficient, which is not included in the model.

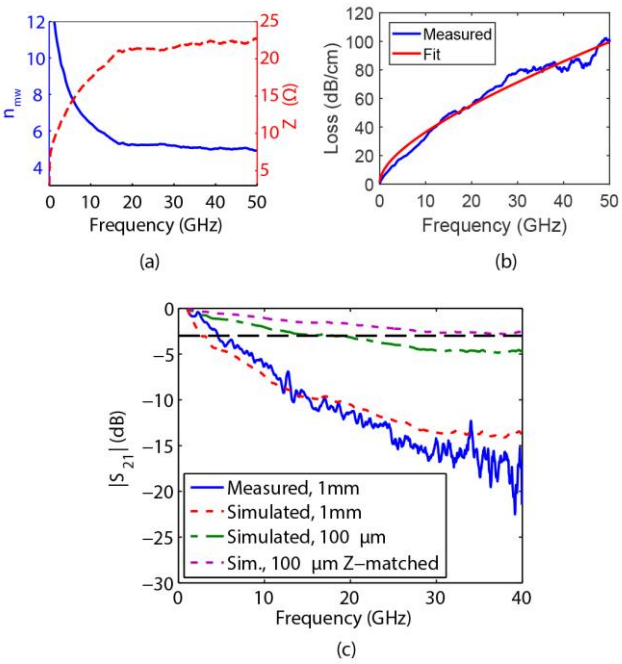

Fig. 3 (a) Measured microwave effective refractive index (n_{mw}) and characteristic impedance (Z) obtained from measured S-parameters. (b) Loss coefficient vs frequency with fitting to $\alpha = \alpha_c\sqrt{f} + \alpha_d f$. (c) Measured (blue solid) and simulated electro-optic frequency response of the modulator. The response is simulated for 1 mm (red dashed) and 100 μm long (green dash-dotted) modulators and for the latter with impedance-matching in the 20-50 GHz region (purple dotted).

The EO frequency response of the modulator can be improved significantly by tailoring the properties of the $BaTiO_3$ PC waveguide and coplanar stripline electrodes. For a $\chi^{(2)}$ PC modulator, the voltage-length product according to an extension of the model proposed by Soljačić et al [15] is

$$V_\pi \cdot L = \frac{\lambda_0 g}{n^2 n_{g,R} f_{eo} r_{eff} \Gamma m(\omega)}. \quad (1)$$

where λ_0 is the free space wavelength, g is the electrode gap spacing, r_{eff} is the effective electro-optic coefficient, Γ is the electro-optic overlap factor, n is the waveguide mode index, $n_{g,R}$ is the group index of the ridge waveguide, and $m(\omega)$ is the value of the electro-optic magnitude response at frequency ω. The electro-optic enhancement factor f_{eo} is given by

$$f_{eo} = (1 - x) + x(n_{g,P}/n_{g,R}), \quad (2)$$

where $x \equiv L_P/L$ is the fractional filling of the interaction region of total length L with a PC of length L_P, and $n_{g,P}$ is the group index of the PC. Details of the derivation of (1) and (2) are given in the Appendix A. The enhancement factor given in (2) is for the case where the enhancement is purely due to the filling fraction of the photonic crystal and the difference in group indices. This is true for the case where the traveling-wave electro-optic frequency response is negligibly affected by the inclusion of the photonic crystal, which is for the case where the phase mismatch is dominated by the other microwave losses and the photonic crystal length and/or group index are small. For our device, the absorption loss is the dominant mechanism and the photonic crystal length is small compared to the total length of the device.

The important result of (1) and (2) is that an increase in the group refractive index of the PC enables a reduction in the

required device length for a π phase shift. Since the microwave losses are length dependent, a smaller footprint enables an increase in the electro-optic bandwidth. To demonstrate, consider a PC device with total length of 100 µm and group refractive index of 20. Using the measured microwave properties of the device reported here and the model of Rahman and Haxha [35] gives the response of the green dash-dot curve in Fig. 3 (c), showing an 18 GHz 3 dB bandwidth. Optimizing the electrode impedance to 50 Ω in the 20-50 GHz region gives the response of the purple dotted curve, which has a 35 GHz 3 dB bandwidth. Both of these devices have a half-wave voltage of 16 V and voltage-length product of 0.16 V-cm for operation at 1550 nm with the same geometry as the device reported here. The half-wave voltage can potentially be reduced to as small as 1.4 V for the 100 µm device by improving the material quality to achieve an effective electro-optic coefficient equal to that of the bulk material (850 pm/V [37]) under high-frequency clamped conditions.

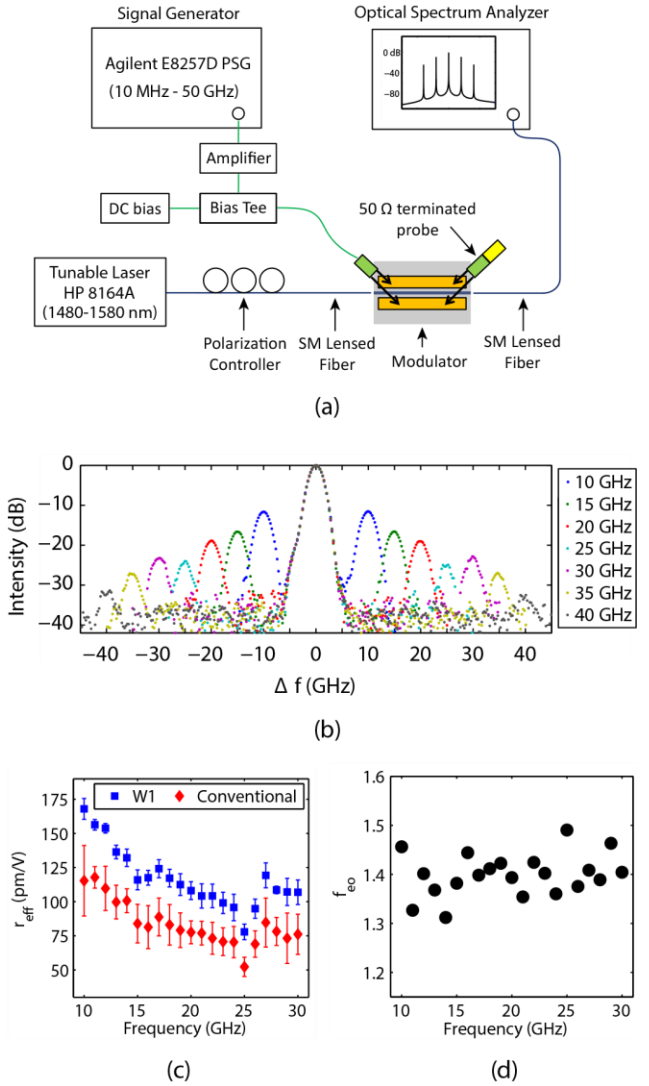

Fig. 4. (a) Experimental setup used to measure the EO phase modulated response. (b) Measured sideband response of the PC modulator for modulation frequencies between 10 and 40 GHz at an optical wavelength of 1530 nm and driving voltage of 5.3 Vpp. (c) Frequency-dependent EO coefficient calculated from the measured sideband response. (d) Frequency-dependent enhancement factor for the total interaction region calculated from the data in (c).

IV. High Frequency Electro-Optic Enhancement

The enhancement of the EO coefficient in the PC waveguide device was measured using optical spectral analysis, a technique for measuring electro-optic device properties in the 10 GHz to 1 THz frequency region [38, 39]. In a previous publication, we demonstrated a device with an optical signal-to-noise ratio (OSNR) of 12 dB at 25 GHz for 2.2 V_{pp} operation through a 25 km fiber and with 8 dB extinction at 50 GHz for 9.1 V_{pp} [40]. Further improvement in the OSNR is expected with optimal design and fabrication process. Advantages of the OSA technique are that figure of merit $V_\pi \cdot L$ can be measured with very low driving voltage and at high frequency. This is in contrast to eye diagram measurement which has its limit both in frequency and extinction ratio. The phase modulated light was detected using an optical spectral analyzer (Yenista OSA20). A schematic of the experimental setup is shown in Fig. 4 (a). Light polarized along the x-direction defined in Fig. 1 (a) (TE polarized light) at 1530 nm wavelength was coupled into the device. A sinusoidal microwave signal with 0 dBm nominal power was amplified by a broadband amplifier to a maximum peak-to-peak voltage of 5.3 V. A DC bias of 10 V was added to the applied signal using a bias tee. While $BaTiO_3$ phase modulators have been demonstrated to operate at much lower bias voltages and fields [34], a bias of 10 V was chosen to sufficiently pole in-plane ferroelectric domains to maximize the electro-optic sideband response.

The measured optical spectra for modulation frequencies between 10 and 40 GHz are plotted in Fig. 4 (b). The data is plotted as intensity versus frequency displacement (Δf) from the center laser wavelength (λ_c). The frequency displacement is calculated as $\Delta f = (c/\lambda^2)(\Delta\lambda)$, where c is the speed of light in free space, λ is the optical wavelength, and $\Delta\lambda = |\lambda - \lambda_c|$. The peak positions are in excellent agreement with the modulation frequency, indicating that they are due to electro-optic phase modulation of TE polarized light.

The effective electro-optic coefficient was measured at modulation frequencies between 10 and 30 GHz using the measured phase modulated response according to the procedure detailed in Appendix B. In brief, the N^{th} order sideband peak intensity is proportional to $J_N^2(z)$, where J_N is the Bessel function of the first kind of order N and z is the phase modulation index given by

$$z = \frac{\omega_0 n^3 r_{eff}}{2c} \Gamma A_{mw} m(\omega) L \tag{3}$$

where ω_0 (ω) is the optical wave's (microwave's) angular frequency, n is the optical mode refractive index, r_{eff} is the effective in-device electro-optic coefficient, c is the speed of light in free space, Γ is the electro-optic overlap factor, A_{mw} is the applied microwave electric field, L is the device length, and $m(\omega)$ is the electro-optic frequency response modeled using the measured frequency-dependent microwave properties. The effective EO coefficient is numerically

calculated from (3) for known values of the sideband peak intensity measured with respect to that of the central peak and known values for all the other parameters. Since the relative peak intensities are required for the measurement, the insertion losses only affect the measurement as the measured signal approaches the noise floor of the OSA, which in our case is -85 dBm. All measurements taken had an OSNR larger than 10 dB to ensure that the sidebands could be clearly distinguished from the noise floor. The level sampling error for the OSA used (Yenista OSA20) is ±0.01 dB, which introduces an error of approximately ±1% for the electro-optic coefficient.

The effective frequency-dependent EO coefficient for the PC modulator and for a conventional modulator that is identical apart from exclusion of the PC are shown in Fig. 4 (c). The error bars correspond to the statistical error obtained from 5 or more measurements at each frequency. The data set includes measurements done on different days which include the effects of fiber realignment to the waveguides. The electro-optic coefficient generally decreases with frequency in the 10-30 GHz range with the sharpest decrease between 10 and 15 GHz. The observed trend of decreasing EO coefficient with frequency follows that of the measured dielectric constant of $BaTiO_3$ thin films [41]. This is not unexpected given the direct relationship between the linear electro-optic coefficient and the dielectric constant tensor elements [42]. For the measurements at 1530 nm with a 5 μm gap spacing, mode refractive index (n) of 2.13, electro-optic overlap factor of 0.71, and electrode length of 1 mm, the voltage-length product for the PC modulator calculated from (1) is 0.66 V-cm and 1.0 V-cm at 10 and 30 GHz, respectively.

A clear enhancement of the effective EO coefficient is observed across the entire frequency range with a calculated enhancement factor between 1.3 and 1.5 (Fig. 4 (d)). The enhancement is beyond the measurement uncertainty, given by the error bars in Fig. 4 (c). The enhancement of the electro-optic coefficient in only the PC region is $f_{eo}^{loc} = n_{g,P}/n_{g,R}$ [43], which according to (2) gives

$$f_{eo}^{loc} = n_g^{PC}/n_g^{wg} = \frac{f_{eo} - (1-x)}{x} \quad (4)$$

Using the measured average enhancement factor of 1.4 and $x = 0.037$ corresponding to a 37 μm long PC in a 1 mm long device, the local enhancement factor is 12. For an intrinsic electro-optic coefficient of 76 pm/V at 30 GHz, the corresponding locally enhanced electro-optic coefficient in the PC region is 900 pm/V. To our knowledge, this is the first quantitative analysis of slow light enhancement of the electro-optic coefficient in a ferroelectric $\chi^{(2)}$ waveguide at microwave frequencies.

V. Wavelength and Voltage Dependent Response

The optical sideband response was also characterized as a function of applied voltage with all other parameters fixed. The voltage-dependent spectra at a modulation frequency of 10 GHz and optical carrier wavelength of 1530 nm are shown for the PC modulator in Fig. 5 (a). The sideband peak intensity increases with applied voltage, which is due to an increase in electro-optic phase delay. The OSNR of the sidebands, defined as the difference between the sideband peak intensity and OSA background, was measured to be 22 dB for 5.3 V_{pp} operation. The phase delay was calculated by taking the ratio of the measured central peak to first order sideband peak intensities and solving numerically for the argument of the Bessel function, as shown in Appendix A [37, 38]. The phase delay calculated using this approach is plotted in Fig. 5 (b) for both the PC and conventional modulators. An enhancement in agreement with that calculated for the electro-optic coefficient is observed across the entire voltage range. Both modulators show a nonlinear dependence of the phase delay on applied voltage. This difference is attributed to the large off-diagonal electro-optic tensor elements $r_{51} = r_{42}$ of the single crystal $BaTiO_3$ film, which adds a quadratic dependence to the voltage-dependent phase delay [44]. The measured phase delay is lower than expected given the electro-optic coefficients calculated in Fig. 4 (c). This is due to the significant attenuation of the microwave field at a modulation frequency of 10 GHz. This can be reduced by either further shortening the electrodes or impedance matching, as previously discussed.

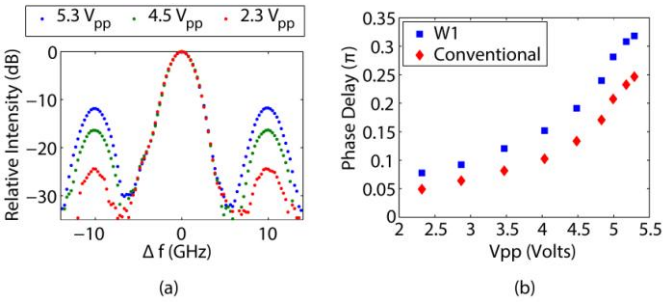

Fig. 5. (a) Measured electro-optic sideband response as a function of applied voltage at 10 GHz. (b) Phase delay versus voltage calculated from the data in (a).

The wavelength-dependent electro-optic device properties were further characterized for TE polarized input light having wavelengths within and below the optical C band (1530-1565 nm). The measured insertion loss due to the PC is 12 dB, obtained by measuring the insertion loss of the same waveguide before and after patterning of the PC. Before patterning the photonic crystal, a total insertion loss of 24 dB was measured for butt coupling to the ridge waveguide with tapered lensed fibers having a spot size of 1.7 μm. The group index scales at least linearly with the group index while the enhancement also scales linearly; hence, there is a trade-off between insertion loss and enhancement. In this work, we chose a relatively short photonic crystal (37 μm) with a moderate group index enhancement in order to unambiguously measure the enhancement with an optical spectrum analyzer. The measured waveguide transmission for TE polarized light is in fair agreement with the transmission simulated using 2D FDTD (Fig. 6 (a)), which has previously been used to successfully describe the transmission of hexagonal lattice PC waveguides on the same $BaTiO_3$ platform in the same wavelength range of interest [32]. The difference in transmission at wavelengths longer than 1530 nm is likely due

to a slightly larger effective mode index of the actual waveguide versus that used for the simulations which was calculated for the unperturbed ridge waveguide structure. The difference in mode index is not expected to significantly otherwise affect the simulated transmission over the narrow 60 nm wavelength range based on reports of other structures with higher index contrast [45]. According to the band diagram of Fig. 2 (a), three crossings between the TE-like defect line mode and TM-like modes are expected between 1500 and 1560 nm. Two regions in the transmission without oscillations at 1540 and 1550 nm possibly correspond to two of these crossings. The frequency shift of these crossing points compared with the band structure of Fig. 2 (a) is likely due to slight differences between the fabricated and simulated hole structures, which has been previously observed on other asymmetric platforms [31]. Clear fringes were measured in the transmission across the entire measurement range. Oscillations with the same fringe spacing were not measured in ridge waveguides on the same wafer, indicating that the fringes are due to Fabry-Perot reflections due to inclusion of the PC cavity. The optical group refractive index (Fig. 6 (b)) was calculated from the fringes as $n_g = \lambda_c^2/(2l_c\Delta\lambda)$, where λ_c is the center wavelength between fringes, l_c is the cavity, and $\Delta\lambda$ is the fringe spacing [46]. The expected period of the oscillations for reflections between the PC and input or output facets is less than 1 nm, hence the oscillations are due to reflections within the PC. Using the length of the W1 segment for l_c, the measured group refractive index is between 15 and 18.

The buffering capacity of slow light waveguides is typically described by the delay-bandwidth product (DBP), defined as $n_g(\Delta\lambda/\lambda)$, where $\Delta\lambda$ is the optical bandwidth over which a group refractive index of $n_g \pm 10\%$ is obtained centered at wavelength λ [47]. For the W1 $BaTiO_3$ waveguide, the corresponding DBP is 0.49. The DBP is believed to be artificially large due to the propagation of light below the PC within the $BaTiO_3$ film and mixing between TE-like and TM-like modes supported by the PC waveguide within the TE bandgap. If the light was confined only to the PC region, then an increase in the group refractive index would be expected as the band edge is approached. This would decrease the optical bandwidth and the corresponding DBP.

Coupling between the TE- and TM-like modes is possible due to the large off-diagonal electro-optic tensor element r_{51} for $BaTiO_3$ [37]. The maximum mode coupling occurs with a periodicity of approximately 6 mm, hence non-negligible coupling occurs in the 1.5 mm long segment between the input facet of the ridge waveguide and the input to the photonic crystal, resulting in both TE and TM polarizations launched into the slow light section. The slow light properties of the TM-like modes are hence expected to additionally contribute to the electro-optic coefficient enhancement. The larger bandwidth covered by the TM-like modes presumably result in the larger than expected bandwidth shown in Fig. 6. Further widening of the bandwidth may be due to imperfections in the photonic crystal fabrication, which, in asymmetric structures, more strongly affect the wavelength dependence of the group index for the TM-like modes [31].

Using the spectral analysis technique, the electro-optic coefficient of the W1 modulator was measured versus wavelength at a modulation frequency of 10 GHz (Fig. 6 (c)). The EO coefficient has a value of 123 pm/V at 1530 nm and decreases to a value of 111 pm/V at 1560 nm. The EO enhancement (Fig. 6 (d)) does not increase across the band edge, as would be expected if the measured group refractive index demonstrated the same trend. Compared with the values in Fig. 4 (c), the effective EO coefficient is lower due to a lower applied peak-to-peak voltage of 4.9 versus 5.3 V. Wideband slow light enhancement with a local enhancement factor of approximately 10 is measured in a 48 nm window centered about 1524 nm (Fig. 6 (d)). This demonstrates the potential use of $\chi^{(2)}$ PC modulators with wideband enhancement for wavelength division multiplexing schemes.

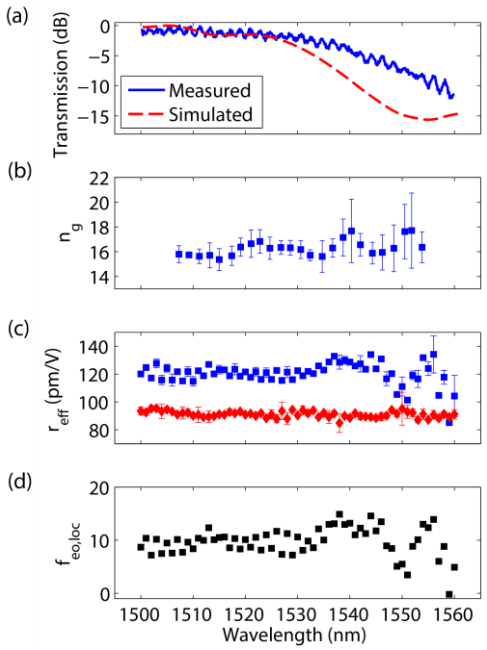

Fig. 6 (a) Measured and simulated transmission versus optical wavelength. (b) Group refractive index calculated from the fringes measured in the transmission. (c) Measured wavelength-dependent EO coefficient for the PC (blue squares) and conventional modulators (red diamond). (d) Wavelength-dependent local enhancement factor calculated from (c) using (4).

VI. Conclusions and Discussion

We demonstrate a $\chi^{(2)}$ electro-optic modulator with a wide optical bandwidth operation at modulation frequencies up to 40 GHz. Slow light EO enhancement is observed over optical wavelengths in the optical C band and at technologically relevant modulation frequencies from 10 to 30 GHz. An EO enhancement factor of 1.4 and an EO coefficient of 107 pm/V at 30 GHz was obtained for a 1 mm long device. A locally enhanced electro-optic coefficient of 900 pm/V was obtained in the photonic crystal region. By exploiting size reduction enabled by the slow light enhancement and impedance matching the electrodes to 50 Ω, devices with electro-optic bandwidths of 40 GHz and voltage-length product of 0.16 V-cm are predicted in devices with a total length of 100 μm. By continuing to improve the quality of the epitaxial films, the voltage-length product can be potentially reduced to 0.014 V-

cm and the device voltage reduced to 1.4 V for a 100 μm long PC device.

We demonstrate an order of magnitude size reduction of $BaTiO_3$ thin film devices is possible via slow light EO enhancement, thereby enabling integration of $\chi^{(2)}$ devices for photonic integrated circuits. The potential for integration with silicon has recently been demonstrated already by others with high quality ferroelectric thin films either epitaxially grown or wafer-bonded to silicon-on-insulator [48-52]. Integrated $\chi^{(2)}$ modulators on silicon could potentially meet the requirements for ultra-high bandwidth modulators in next generation telecommunication and data center systems and could also serve as important components for quantum optical communications [53]. Furthermore high sensitivity electromagnetic field sensors could be potentially realized [54]. Using the approach of slow light PC waveguides on ferroelectric $\chi^{(2)}$ thin films reported here, compact, efficient, and high speed modulators for both classical and quantum optical information processing applications are envisioned.

APPENDIX A
ELECTRO-OPTIC COEFFICIENT ENHANCEMENT IN $\chi^{(2)}$ WAVEGUIDES

The phase delay in a waveguide with high group index is, in the most general sense, given by [14]

$$\delta\phi = \frac{2\pi L}{\lambda_0}\Gamma\frac{\delta n}{n}n_g, \tag{A1}$$

where $\delta\phi$ is the total phase delay, L is the interaction length, λ_0 is the optical wavelength in free space, n is the optical index, δn is the modulation of the refractive index, and Γ is the fraction of optical power confined in the region which experiences a refractive index change δn due to an applied external stimulus. For the case of an electro-optic material where the applied stimulus is an electric field, the refractive index change is given by

$$\delta n = \frac{1}{2}n^3 r_{eff}\frac{Vm(\omega)}{g}, \tag{A2}$$

where r_{eff} is the effective EO coefficient representing the overall contribution from the electro-optic tensor elements, and V is the applied voltage across a gap spacing g, and $m(\omega)$ is the electro-optic magnitude response at the microwave modulation angular frequency ω. Substituting (A2) into (A1) gives the general relation for the phase shift in a $\chi^{(2)}$ waveguide due to the electro-optic effect:

$$\delta\phi = \frac{\pi L}{\lambda_0}\Gamma m(\omega)n^2 n_g r_{eff}\frac{V}{g}. \tag{A3}$$

Here, we consider the reduction in voltage-length product and enhancement of the electro-optic coefficient for $\chi^{(2)}$ modulators. The approach is generalized for a PC modulator having a total interaction length L within which a PC of length L_P is placed. The length of the interaction region without the photonic crystal is $L_R = L - L_P$. The total phase delay in the ridge waveguide region without the photonic crystal is

$$\delta\phi_R = \frac{\pi L_R}{\lambda_0}\Gamma m(\omega)n^2 n_{g,R} r_{eff}\frac{V}{g}, \tag{A4}$$

where $n_{g,R}$ is the group index of the ridge waveguide. The phase delay in the photonic crystal segment is given similarly by

$$\delta\phi_P = \frac{\pi L_P}{\lambda_0}\Gamma m(\omega)n^2 n_{g,P} r_{eff}\frac{V}{g}. \tag{A5}$$

The total phase delay $\delta\phi_T$ in the composite ridge and photonic crystal waveguide is then $\delta\phi_T = \delta\phi_R + \delta\phi_P$ or

$$\delta\phi_T = \frac{\pi}{\lambda_0}\Gamma m(\omega)n^2 r_{eff}\frac{V}{g}(n_{g,R}L_R + n_{g,P}L_P). \tag{A6}$$

Using (A6), the half-wave voltage of the composite waveguide modulator is obtained by setting $\delta\phi_T = \pi$ and solving for the voltage:

$$V_\pi = \frac{\lambda_0 g}{n^2 r_{eff}\Gamma m(\omega)L}\left[(1-x)n_{g,R} + xn_{g,P}\right]^{-1} \tag{A7}$$

where $x \equiv L_P/L$. Solving for the voltage-length product $V_\pi \cdot L$ gives

$$V_\pi \cdot L = \frac{\lambda_0 g}{n^2 r_{eff}\Gamma m(\omega)}\left[(1-x)n_{g,R} + xn_{g,P}\right]^{-1} \tag{A8}$$

For the case of a conventional modulator where $L_P = 0$, the voltage-length product reduces to

$$V_\pi \cdot L = \frac{\lambda_0 g}{n^2 n_{g,R} r_{eff}\Gamma m(\omega)}. \tag{A9}$$

Comparing (A8) and (A9), the effective EO coefficient is enhanced in the composite waveguide modulator by the factor

$$f_{eo} = (1-x) + x(n_{g,P}/n_{g,R}). \tag{A10}$$

The voltage-length product of a photonic crystal modulator can hence be written generally as

$$V_\pi \cdot L = \frac{\lambda_0 g}{n^2 n_{g,R} f_{eo} r_{eff}\Gamma m(\omega)}. \tag{A11}$$

APPENDIX B
MEASUREMENT OF THE HIGH-FREQUENCY EO COEFFICIENT VIA OPTICAL SPECTRAL ANALYSIS

The optical spectrum of laser light with center angular frequency ω_0 that is phase modulated at a microwave angular frequency ω_{mw} is given by

$$I(\omega) \propto \sum_{N=-\infty}^{\infty} J_N^2(z)\delta(\omega_0 - \omega - N\omega_{mw}) \tag{A12}$$

where $J_N(z)$ is the Bessel function of the first kind of order N, ω is the light angular frequency, and $\delta(\omega)$ is the Dirac delta function. The argument of the Bessel function is

$$z = \frac{\omega_0 n^3 r_{eff}}{2c}\Gamma A_{mw} m(f) L \tag{A13}$$

The theoretical response is a series of peaks distributed equidistantly on either side of the center laser angular frequency ω_0 with separation distance equal to an N^{th} order of the modulation angular frequency ω_{mw}. The variables in (A13) are defined in the main text following (3). The intensity of the N order sideband peak is given by $J_N^2(z)$, which is a function of r_{eff}. Hence, from a given measured spectrum, numerically solving

$$\frac{J_1^2(z)}{J_0^2(z)} = \frac{I(\omega_0 + \omega_{mw})}{I(\omega_0)} \tag{A14}$$

for z and applying (A13) gives the measured r_{eff}.

ACKNOWLEDGMENT

The authors acknowledge enlightening discussions and modeling assistance from C. Husko and technical assistance

with focused ion beam fabrication from I. W. Jung and L. Ocola, Argonne National Labs.

Peter Girouard received his B.S. in mechanical engineering (2012) and M.S. in materials science and engineering (2012) from Boston University and his PhD in materials science and engineering from Northwestern University (2016). He is currently a post-doctoral researcher at the Technical University of Denmark where he is working on silicon-based nonlinear optical material platforms for integrated photonics.

Young Kyu Jeong received his Ph.D. degree in Materials Science and Engineering in Pohang University of Science and Technology (POTECH), Pohang, Korea, in 2011. He is currently a Research Associate at Korea Institute of Industrial Technology (KITECH), Republic of Korea. His research interests include various oxide systems including ferroelectrics, ferromagnetic materials and spintronics.

Pice Chen received his Ph.D. degree in Materials Science in University of Wisconsin-Madison in 2013. He then joined Northwestern University as a postdoctoral research associate, focusing on developing high-frequency electro-optic devices based on heteroepitaxial ferroelectric thin films. He is currently a postdoctoral research associate at Argonne National Laboratory. His research interests include ultrafast synchrotron x-ray scattering, ferroelectric and piezoelectric materials, and electronic and photonic devices.

Zhifu Liu received the B.S. degree in physics from Lanzhou University in 1983, and the Ph.D. degree in physics from Alabama A&M University, Huntsville, AL in 2001. He is currently a Research Assistant Professor in the Department of Materials Science and Engineering, Northwestern University, Evanston, IL. His research areas include integrated optics, thin film optics, and compound semiconductors for radiation detection.

Seng-Tiong Ho (S'83–M'89) received the B.S., M.S., and Ph.D. degrees in electrical engineering from the Massachusetts Institute of Technology, Cambridge, in 1984 and 1989, respectively.

From 1989 to 1992, he was a Member of Technical Staff at AT&T Bell Laboratories, Murray Hill, NJ. Since 1991, he has been a Faculty Member in the Department of Electrical Engineering and Computer Science, Northwestern University, Evanston, IL. His research areas include nanophotonics, microcavity lasers, quantum phenomena in low-dimensional photonic structures, nanofabrication, ultrafast nonlinear optical phenomena, electrooptic modulators, optical communications, and quantum optics.

Prof. Ho is a Fellow of the Optical Society of America.

Bruce W. Wessels received the B.S. degree from the University of Pennsylvania, Philadelphia, and the Ph.D. degree in materials science from the Massachusetts Institute of Technology, Cambridge.

He was a Member of Technical Staff of the General Electric Research and Development Center. He joined the faculty of McCormick School of Engineering, Northwestern University, Evanston, IL, where he is currently a W. P. Murphy Professor of Materials Science and Electrical Engineering and Computer Science. His research interests include the electronic, magnetic and optical properties of semiconductor and dielectric materials and devices.

Prof. Wessels is a fellow of OSA, APS, TMS and ASMI.

REFERENCES

[1] D. A. Miller, "Device requirements for optical interconnects to silicon chips," *Proceedings of the IEEE*, vol. 97, no. 7, pp. 1166-1185, Jul. 2009.

[2] E. L. Wooten, K. M. Kissa, A. Yi-Yan, E. J. Murphy, D. Lafaw, P. F. Hallemeier, D. Maack, D. V. Attanasio, D. J. Fritz, and G. J. McBrien, "A review of lithium niobate modulators for fiber-optic communications systems," *Selected Topics in Quantum Electronics, IEEE Journal of*, vol. 6, no. 1, pp. 69-82, Jan.-Feb. 2000.

[3] G. T. Reed, G. Mashanovich, F. Gardes, and D. Thomson, "Silicon optical modulators," *Nature Photonics*, vol. 4, no. 8, pp. 518-526, Aug. 2010.

[4] Q. Huang, Y. Wu, K. Ma, J. Zhang, W. Xie, X. Fu, Y. Shi, K. Chen, J.-J. He, D. Van Thourhout, G. Roelkens, L. Liu, and S. He, "Low driving voltage band-filling-based III-V-on-silicon electroabsorption modulator," *Applied Physics Letters*, vol. 108, no. 14, pp. 141104, Apr. 2016.

[5] M. Roussey, M.-P. Bernal, N. Courjal, D. Van Labeke, F. Baida, and R. Salut, "Electro-optic effect exaltation on lithium niobate photonic crystals due to slow photons," *Applied Physics Letters*, vol. 89, no. 24, pp. 241110, Dec. 2006.

[6] M. Roussey, F. I. Baida, and M.-P. Bernal, "Experimental and theoretical observations of the slow-light effect on a tunable photonic crystal," *Journal of the Optical Society of America B*, vol. 24, no. 6, pp. 1416-1422, Jun. 2007.

[7] H. Lu, B. Sadani, G. Ulliac, N. Courjal, C. Guyot, J. M. Merolla, M. Collet, F. I. Baida, and M. P. Bernal, "6-micron interaction length electro-optic modulation based on lithium niobate photonic crystal cavity," *Optics Express*, vol. 20, no. 19, pp. 20884-20893, Sep. 2012.

[8] H. Lu, B. Sadani, N. Courjal, G. Ulliac, N. Smith, V. Stenger, M. Collet, F. Baida, and M.-P. Bernal, "Enhanced electro-optical lithium niobate photonic crystal wire waveguide on a smart-cut thin film," *Optics Express*, vol. 20, no. 3, pp. 2974-2981, Jan. 2012.

[9] F. Sulser, G. Poberaj, M. Koechlin, and P. Günter, "Photonic crystal structures in ion-sliced lithium niobate thin films," *Optics Express*, vol. 17, no. 22, pp. 20291-20300, Oct. 2009.

[10] H. C. Nguyen, S. Hashimoto, M. Shinkawa, and T. Baba, "Compact and fast photonic crystal silicon optical modulators," *Optics Express*, vol. 20, no. 20, pp. 22465-22474, Sep. 2012.

[11] A. Brimont, D. Thomson, F. Gardes, J. Fedeli, G. Reed, J. Martí, and P. Sanchis, "High-contrast 40 Gb/s operation of a 500 μm long silicon carrier-depletion slow wave modulator," *Optics Letters*, vol. 37, no. 17, pp. 3504-3506, Sep. 2012.

[12] A. Brimont, D. Thomson, P. Sanchis, J. Herrera, F. Gardes, J. Fedeli, G. Reed, and J. Martí, "High speed silicon electro-optical modulators enhanced via slow light propagation," *Optics Express*, vol. 19, no. 21, pp. 20876-20885, Oct. 2011.

[13] L. Gu, W. Jiang, X. Chen, L. Wang, and R. T. Chen, "High speed silicon photonic crystal waveguide modulator for low voltage operation," *Applied Physics Letters*, vol. 90, no. 7, pp. 071105, Feb. 2007.

[14] K. Hojo, Y. Terada, N. Yazawa, T. Watanabe, and T. Baba, "Compact QPSK and PAM Modulators With Si Photonic Crystal Slow-Light Phase Shifters," *IEEE Photonics Technology Letters*, vol. 28, no. 13, pp. 1438-1441, Jul. 2016.

[15] M. Soljačić, S. G. Johnson, S. Fan, M. Ibanescu, E. Ippen, and J. Joannopoulos, "Photonic-crystal slow-light enhancement of nonlinear phase sensitivity," *JOSA B*, vol. 19, no. 9, pp. 2052-2059, Sep. 2002.

[16] X. Zhang, A. Hosseini, S. Chakravarty, J. Luo, A. K.-Y. Jen, and R. T. Chen, "Wide optical spectrum range, subvolt, compact modulator based on an electro-optic polymer refilled silicon slot photonic crystal waveguide," *Optics Letters*, vol. 38, no. 22, pp. 4931-4934, Nov. 2013.

[17] X. Zhang, C.-J. Chung, A. Hosseini, H. Subbaraman, J. Luo, A. Jen, R. Neilson, C. Lee, and R. T. Chen, "High performance optical modulator based on electro-optic polymer filled silicon slot photonic crystal

waveguide," *Journal of Lightwave Technology*, vol. 34, no. 12, pp. 2941-2951, Jun. 2016.
[18] J. H. Wülbern, J. Hampe, A. Petrov, M. Eich, J. Luo, A. K.-Y. Jen, A. Di Falco, T. F. Krauss, and J. Bruns, "Electro-optic modulation in slotted resonant photonic crystal heterostructures," *Applied Physics Letters*, vol. 94, no. 24, pp. 241107, Jun. 2009.
[19] S.-I. Inoue and A. Otomo, "Electro-optic polymer/silicon hybrid slow light modulator based on one-dimensional photonic crystal waveguides," *Applied Physics Letters*, vol. 103, no. 17, pp. 171101, Oct. 2013.
[20] P. Tang, A. L. Meier, D. J. Towner, and B. W. Wessels, "$BaTiO_3$ thin-film waveguide modulator with a low voltage-length product at near-infrared wavelengths of 0.98 and 1.55 μm," *Optics Letters*, vol. 30, no. 3, pp. 254-256, Feb. 2005.
[21] P. Girouard, P. Chen, Y. Tu, Y. K. Jeong, Z. Liu, S.-T. Ho, and B. W. Wessels, "Ultrahigh Bandwidth, Low V_π Photonic Crystal $BaTiO_3$ Modulators," in *Integrated Photonics Research, Silicon and Nanophotonics*, 2015, p. IM2B. 4.
[22] M. Streshinsky, R. Ding, Y. Liu, A. Novack, Y. Yang, Y. Ma, X. Tu, E. K. S. Chee, A. E.-J. Lim, P. G.-Q. Lo, T. Baehr-Jones, and M. Hochberg, "Low power 50 Gb/s silicon traveling wave Mach-Zehnder modulator near 1300 nm," *Optics Express*, vol. 21, no. 25, pp. 30350-30357, Dec. 2013.
[23] P. Girouard, P. Chen, Y. K. Jeong, Z. Liu, and B. W. Wessels, "Microwave Properties of $BaTiO_3$ Modulators for Integrated Photonics," *(in preparation)*, 2017.
[24] J. Li, Z. Liu, Y. Tu, S.-T. Ho, I. W. Jung, L. E. Ocola, and B. W. Wessels, "Photonic Crystal Waveguide Electro-Optic Modulator With a Wide Bandwidth," *Journal of Lightwave Technology*, vol. 31, no. 10, pp. 1601-1607, May. 2013.
[25] D. J. Towner, J. Ni, T. J. Marks, and B. W. Wessels, "Effects of two-stage deposition on the structure and properties of heteroepitaxial $BaTiO_3$ thin films," *Journal of Crystal Growth*, vol. 255, no. 1, pp. 107-113, Jul. 2003.
[26] Y. K. Jeong and B. W. Wessels, "Properties of epitaxial barium titanate thin films using a highly volatile Ba (hfa) 2triglyme precursor," *Journal of Vacuum Science & Technology B*, vol. 33, no. 5, p. 051206, Sep. 2015.
[27] S. Olivier, M. Rattier, H. Benisty, C. Weisbuch, C. Smith, R. De La Rue, T. Krauss, U. Oesterle, and R. Houdré, "Mini-stopbands of a one-dimensional system: The channel waveguide in a two-dimensional photonic crystal," *Physical Review B*, vol. 63, no. 11, pp. 113311, Mar. 2001.
[28] G. Burr, S. Diziain, and M.-P. Bernal, "The impact of finite-depth cylindrical and conical holes in lithium niobate photonic crystals," *Optics Express*, vol. 16, no. 9, pp. 6302-6316, Apr. 2008.
[29] C. Monat, B. Corcoran, M. Ebnali-Heidari, C. Grillet, B. J. Eggleton, T. P. White, L. O'Faolain, and T. F. Krauss, "Slow light enhancement of nonlinear effects in silicon engineered photonic crystal waveguides," *Optics Express*, vol. 17, no. 4, pp. 2944-2953, Feb. 2009.
[30] M. Qiu, "Band gap effects in asymmetric photonic crystal slabs," *Physical Review B*, vol. 66, no. 3, p. 033103, Jul. 2002.
[31] Y. A. Vlasov, N. Moll, and S. J. McNab, "Mode mixing in asymmetric double-trench photonic crystal waveguides," *Journal of Applied Physics*, vol. 95, no. 9, pp. 4538-4544, May. 2004.
[32] P. Girouard, P. Chen, Y. Tu, Y. K. Jeong, Z. Liu, S.-T. Ho, and B. W. Wessels, "Small Footprint Barium Titanate Photonic Crystal Modulators for Photonic Integrated Circuits," in *Conference on Lasers and Electro-Optics*, San Jose, California, 2015, p. SW4I.5.
[33] K. Noguchi, H. Miyazawa, and O. Mitomi, "Frequency-dependent propagation characteristics of coplanar waveguide electrode on 100GHz Ti: $LiNbO_3$ optical modulator," *Electronics Letters*, vol. 34, no. 7, pp. 661-663, Apr. 1998.
[34] P. Tang, A. Meier, D. Towner, and B. Wessels, "High-speed travelling-wave $BaTiO_3$ thin-film electro-optic modulators," *Electronics Letters*, vol. 41, no. 23, pp. 1296-1297, Nov. 2005.
[35] S. Haxha, B. Rahman, and K. T. Grattan, "Bandwidth estimation for ultra-high-speed lithium niobate modulators," *Applied Optics*, vol. 42, no. 15, pp. 2674-2682, May. 2003.
[36] P. Tang, D. Towner, T. Hamano, A. Meier, and B. Wessels, "Electrooptic modulation up to 40 GHz in a barium titanate thin film waveguide modulator," *Optics Express*, vol. 12, no. 24, pp. 5962-5967, Nov. 2004.
[37] A. Yariv and P. Yeh, *Optical Waves in Crystals*. New York, NY: Wiley, 1984.
[38] Y. Shi, L. Yan, and A. E. Willner, "High-Speed Electrooptic Modulator Characterization Using Optical Spectrum Analysis," *Journal of Lightwave Technology*, vol. 21, no. 10, pp. 2358-2367, Oct. 2003.
[39] M. Lee, H. E. Katz, C. Erben, D. M. Gill, P. Gopalan, J. D. Heber, and D.J. McGee, "Broadband modulation of light by using an electro-optic polymer," *Science*, vol. 298, no. 5597, pp. 1401-1403, Nov. 2002.
[40] Peter Girouard, Pice Chen, Young Kyu Jeong, Zhifu Liu, Seng-Tiong Ho, and Bruce W. Wessels, "Integrated $BaTiO_3$ Modulator with 8 dB Extinction at 50 GHz and 25 km Reach," WC7, in *IEEE InterConnect Conference*, IEEE (2016).
[41] T. Hamano, D. Towner, and B. Wessels, "Relative dielectric constant of epitaxial $BaTiO_3$ thin films in the GHz frequency range," *Applied Physics Letters*, vol. 83, no. 25, pp. 5274-5276, Dec. 2003.
[42] M. DrDomenico Jr and S. Wemple, "Oxygen-octahedra ferroelectrics. I. Theory of electro-optical and nonlinear optical effects," *Journal of Applied Physics*, vol. 40, no. 2, pp. 720-734, Feb. 1969.
[43] R. S. Jacobsen, K. N. Andersen, P. I. Borel, J. Fage-Pedersen, L. H. Frandsen, O. Hansen, M. Kristensen, A. V. Lavrinenko, G. Moulin, and H. Ou,"Strained silicon as a new electro-optic material," *Nature*, vol. 441, no. 7090, pp. 199-202, May. 2006.
[44] M. Aillerie, N. Theofanous, and M. Fontana, "Measurement of the electro-optic coefficients: description and comparison of the experimental techniques," *Applied Physics B*, vol. 70, no. 3, pp. 317-334, Mar. 2000.
[45] M. Qiu, "Effective index method for heterostructure-slab-waveguide-based two-dimensional photonic crystals," *Applied Physics Letters*, vol 81, no. 7, pp. 1163-1165, Aug. 2002.
[46] M. Notomi, K. Yamada, A. Shinya, J. Takahashi, C. Takahashi, and I. Yokohama, "Extremely large group-velocity dispersion of line-defect waveguides in photonic crystal slabs," *Physical Review Letters*, vol. 87, no. 25, p. 253902, Nov. 2001.
[47] F.-C. Leng, W.-Y. Liang, B. Liu, T.-B. Wang, and H.-Z. Wang, "Wideband slow light and dispersion control in oblique lattice photonic crystal waveguides," *Optics Express*, vol. 18, no. 6, pp. 5707-5712, Mar. 2010.
[48] C. Xiong, W. H. P. Pernice, J. H. Ngai, J. W. Reiner, D. Kumah, F. J. Walker, C. H. Ahn, and H. X. Tang, "Active Silicon Integrated Nanophotonics: Ferroelectric $BaTiO_3$ Devices," *Nano Letters*, vol. 14, no. 3, pp. 1419-1425, Feb. 2014.
[49] S. Abel, T. Stöferle, C. Marchiori, C. Rossel, M. D. Rossell, R. Erni, D. Caimi, M. Sousa, A. Chelnokov, B. J. Offrein, and J. Fompeyrine, "A strong electro-optically active lead-free ferroelectric integrated on silicon," *Nature Communications*, vol. 4, pp. 1671, Apr. 2013.
[50] L. Chen, Q. Xu, M. G. Wood, and R. M. Reano, "Hybrid silicon and lithium niobate electro-optical ring modulator," *Optica*, vol. 1, no. 2, pp. 112-118, Aug. 2014.
[51] L. Cai, H. Han, S. Zhang, H. Hu, and K. Wang, "Photonic crystal slab fabricated on the platform of lithium niobate-on-insulator," *Optics Letters*, vol. 39, no. 17, pp. 1367-1369, Sep. 2001.
[52] Y. S. Lee, G.-D. Kim, W.-J. Kim, S.-S. Lee, W.-G. Lee, and W. H. Steier, "Hybrid Si-$LiNbO_3$ microring electro-optically tunable resonators for active photonic devices," *Optics Letters*, vol. 36, no. 7, pp. 1119-1121, Apr. 2011.
[53] K. Banaszek, A. B. U'Ren, and I. A. Walmsley, "Generation of correlated photons in controlled spatial modes by downconversion in nonlinear waveguides," *Optics Letters*, vol. 26, no. 17, pp. 1367-1369, Sep. 2001.
[54] Zhang, Xingyu, Amir Hosseini, Harish Subbaraman, Shiyi Wang, Qiwen Zhan, Jingdong Luo, Alex K-Y. Jen, and Ray T. Chen , "Integrated Photonic Electromagnetic Field Sensor Based on Broadband Bowtie Antenna Coupled Silicon Organic Hybrid Modulator," *Journal of Lightwave Technology* , vol.32, no.20, pp.3774-3784 (2014).